PROCEEDINGS OF SPIE

SPIEDigitalLibrary.org/conference-proceedings-of-spie

Characterization of a PVDF sensor embedded in a metal structure using ultrasonic additive manufacturing

Mohid Khattak, Leon Headings, Marcelo Dapino

Mohid M. Khattak, Leon M. Headings, Marcelo J. Dapino, "Characterization of a PVDF sensor embedded in a metal structure using ultrasonic additive manufacturing," Proc. SPIE 12489, NDE 4.0, Predictive Maintenance, Communication, and Energy Systems: The Digital Transformation of NDE, 124890F (25 April 2023); doi: 10.1117/12.2659270

SPIE.

Event: SPIE Smart Structures + Nondestructive Evaluation, 2023, Long Beach, California, United States

Downloaded From: https://www.spiedigitallibrary.org/conference-proceedings-of-spie on 23 May 2023 Terms of Use: https://www.spiedigitallibrary.org/terms-of-use

Characterization of a PVDF sensor embedded in a metal structure using ultrasonic additive manufacturing

Mohid M. Khattak[1], Leon M. Headings[1], and Marcelo J. Dapino[1]

[1]NSF IUCRC Smart Vehicle Concepts Center, Department of Mechanical and Aerospace Engineering, The Ohio State University, Columbus, OH, USA

ABSTRACT

This paper investigates the characterization and functional performance of a piezoelectric polyvinylidene fluoride (PVDF) sensor embedded into an aluminum plate using ultrasonic additive manufacturing (UAM). While conventional manufacturing techniques such as non-resin-based powder metallurgy are being used to surface-mount smart materials to metals, they pose their own set of problems. Standard manufacturing approaches can physically damage the sensor or deteriorate electrochemical properties of the active material due to high processing temperatures or long adhesive settling times. In contrast, UAM integrates solid-state metal joining with subtractive processes to enable the fabrication of smart structures by embedding sensors, actuators, and electronics in metal-matrices without thermal loading. In this paper, a commercial PVDF sensor is embedded in aluminum with a pre-compression to provide frictional coupling between the sensor and the metal-matrix, thus eliminating the need for adhesives. Axial impact and bending (shaker) tests are conducted on the specimen to characterize the PVDF sensor's frequency bandwidth and impact detection performance. Metal-matrices with active components have been under investigation to functionalize metals for various applications including aerospace, automotive, and biomedical. UAM embedment of sensors in metals enables functionalization of structures for measurement of stresses and temperature within the structure while also serving to shield smart components from environmental hazards. This technique can serve a wide-range of applications including robotics and tactile sensing, energy harvesting, and structural health monitoring.

Keywords: Active metal matrix, embedded sensor, ultrasonic additive manufacturing, piezoelectric PVDF sensor, non-destructive testing

1. INTRODUCTION

Over the last decade, increase in connectivity among systems and introduction of smart automation has introduced the concept of industry 4.0. This fourth industrial revolution aims to bridge the gap between digitization and physical operations of systems and to create tools to design, control, and manufacture cyber-physical systems. Traditional manufacturing techniques combined with modern tools for inter-machine communication have given rise to contemporary industrial practices which make use of the internet-of-things (IoT) to integrate real-time data.[1,2] This enables such smart machines to analyze their performance concurrently, which not only increases their efficiency but also helps to enable system diagnosis with little or no human intervention.[3] Embedded sensors play an important part in this application for actual data retrieval and process optimization through in-situ monitoring and automation.

Conventional embedment of sensors utilizing traditional manufacturing processes present a variety of limitations. Hu et al.[4] and Gayakwad[5] investigated embedment of lead zirconate titanate (PZT) ceramic patches within concrete cylinders for structural health monitoring (SHM) of civil infrastructures. Wang et al. worked on embedding a PZT sensor in a polymethyl methacrylate (PMMA) tube filled with epoxy resins for damage quantification in metals.[6] Other studies focused on embedding piezoelectric sensors in reinforced-fiber and other types of composites for damage detection in lightweight structures.[7–10] Grandal et al.[11] analyzed embedded fiber optic sensors in metals while Hossain[12] studied the effect of embedded piezoceramic sensors in an alumina housing. Although various methods have been adopted to embed sensors in a parent matrix for diagnostic purposes,

Further author information: (Send correspondence to Marcelo J. Dapino)
E-mail: dapino.1@osu.edu

NDE 4.0, Predictive Maintenance, Communication, and Energy Systems: The Digital Transformation of NDE, edited by Norbert G. Meyendorf, Christopher Niezrecki, Ripi Singh, Proc. of SPIE Vol. 12489, 124890F · © 2023 SPIE · 0277-786X · doi: 10.1117/12.2659270

Downloaded From: https://www.spiedigitallibrary.org/conference-proceedings-of-spie on 23 May 2023
Terms of Use: https://www.spiedigitallibrary.org/terms-of-use

these traditional methodologies typically require high processing temperatures or metal deposition techniques. Piezoelectric materials tend to have low Curie points and hence are susceptible to damage due to high processing temperatures in addition to specific mechanical failure modes such as shear (in the case of piezoceramics) and puncture (in the case of films). Additionally, the power and conditioning electronics associated with these sensors require a robust housing for damage prevention. Researchers have used fastening or molding techniques to embed piezoelectric sensors in different materials via adhesives such as epoxy[13,14] or silicone elastomers.[15,16] Not only do these involve prolonged curing times but also interfere with the response of the sensors due to the bonding medium.[17]

Limited work has been done on embedding piezoelectric sensors in metal matrices through low-temperature manufacturing processes. Ramanathan et al. investigated the use of ultrasonic additive manufacturing (UAM) to embed polyvinylidene fluoride (PVDF) sensors in an aluminum structure.[18] UAM, or ultrasonic consolidation, is a solid-state process that utilizes ultrasonic metal welding to additively join metal foils using ultrasonic vibrations in conjunction with normal force; state-of-the-art UAM equipment is integrated with computer numerical control (CNC) machining to enable automated additive and subtractive operations. The process consists of a rolling sonotrode that vibrates ultrasonically giving rise to high plastic flow at the interface between the foil being welded and the substrate. This ensures a solid-state bond between metal foils causing them to coalesce.[19] This methodology has been used to create multi-material structures with embedded active sensors such as shape memory alloys (SMA)[20,21] for actuation purposes, electrical circuitry[22] and fiber optic sensors for SHM purposes.[23]

Hahnlen and Dapino have shown that the temperature of the welding surface during UAM stays below the curie temperature of PVDF which ensures its sensing capabilities.[24] Furthermore, due to its concurrent use with CNC operations, UAM can be used to manufacture the required geometry for successful embedment of sensors without the detrimental effects of temperature-intensive processes. Ramanathan et al. explored a process to embed PVDF sensors in a metal matrix by milling a cavity in the baseplate for the sensor and wires needed for retrieval of real-time sensor data, then ultrasonically welding a layer of foil over the sensor.[18] A pre-compression of the sensor, defined by the pocket depth, effectively strains the PVDF and provides mechanical coupling between the sensor and metal matrix. Even though the process showed promising results with respect to specimen sensitivity, there still remained areas for improvement which needed further exploration. This paper focuses on these improvements and aims to further characterize the embedded PVDF sensor. A similar specimen is developed and exposed to impact and bending (shaker) tests to delineate its frequency bandwidth and impact detection performance.

2. FABRICATION OF SENSOR SPECIMEN

Fabrication of the sensor specimen is achieved by embedding a PVDF sensor in the metal structure, as shown in Figure 1a. This embedment is aided by pre-compressing the PVDF film through welding of two aluminum foils on top. The PVDF film exhibits high voltage constant and layers of polyamide (Kapton) tape, which add to its toughness, are used to laminate the sensor and avoid damage from the scrubbing action between the foil and metal structure as part of the UAM process. The Kapton tapes also insulate the sensor electrodes from the metal matrix around it thus ensuring adequate electrical response. A 12 μm pre-compression thickness has been experimentally shown to be adequate.[18] Sensor and pocket dimensions, and channel depth can be seen in Figure 1b.

The sensor is first etched out on a 40 μm thick sheet with sputtered silver electrodes on both sides. Acetone is used to remove the electrode around the effective sensor area, which is cut with a razor blade to the specified dimensions. Copper tape is cut into two 1 mm wide by 10 mm long electrical leads, which are attached to the electrodes such that 5 mm extends from the sensor. The sensor is then sandwiched between two 50 μm Kapton sheets on top and one on the bottom to provide electrical isolation and mechanical protection. Insulated electrical wires are soldered on the exposed regions of the copper leads which are then wrapped with electrical tape to prevent shorting. Thus, the sensor has an effective active area of 40 mm $\times$ 2.5 mm $\times$ 190 μm.

The weld area on an Al 6061-T6 baseplate is textured by running the UAM sonotrode over the area without a foil. This imparts the sonotrode's texture to the surface which improves subsequent foil welding. An Al 6061-H18 foil is welded over this area to provide a strong weld to the baseplate. Required pockets are milled into the

Downloaded From: https://www.spiedigitallibrary.org/conference-proceedings-of-spie on 23 May 2023
Terms of Use: https://www.spiedigitallibrary.org/terms-of-use

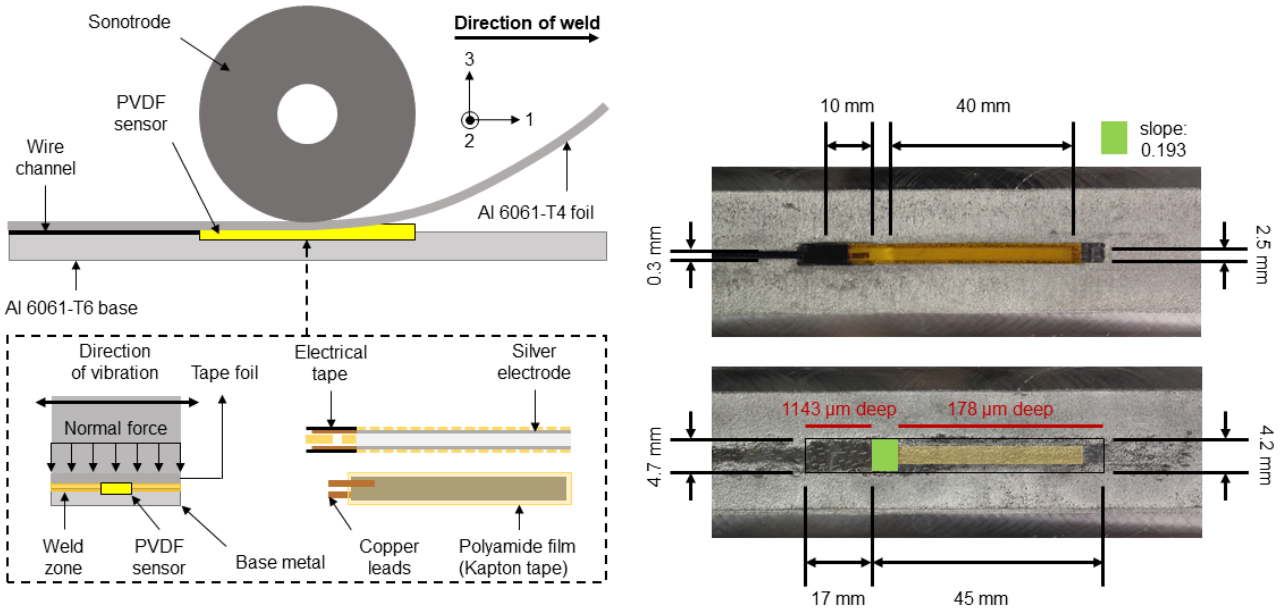

(a) (b)

Figure 1: (a) Schematic embedment of a polyamide-clad PVDF sensor between aluminium foil and a baseplate through ultrasonic additive manufacturing (UAM). The cross-sectional view displays the compression forces exerted by the sonotrode on the sensor. (b) Sensor and pocket dimensions after tacking and milling respectively.

baseplate along with a wire channel to route the sensor wiring. The pocket for the wire connections is milled deeper than the active sensing area pocket depth to ensure pre-compression of the PVDF sensor without damage to the connections. A sloped transition is introduced between the two channel depths in order to provide bending stress relief to the electrical connections. The PVDF sensor is then lightly tacked inside the milled pockets with an adhesive to hold it in place during the UAM process; a depth gauge is used to ensure that the top surface of the sensor is above the top surface of the aluminum baseplate. Two Al 6061-T4 tape foils are then welded over the sensor area and compression is verified by observing the texture imparted over the sensing area. This texture can only be introduced if an opposing force is pushing against the welded tape. Furthermore, the capacitance of the embedded sensor post welding is validated to be 0.35 nF and its resistance to be on the order of mega Ohms. This confirms that the sensor is insulated from the metal matrix and that there is no electrical short. Lastly, wires from the sensor are folded out of the way and the specimen is milled on the CNC into a rectangular beam which has standardized ASTM D638 type-1 dimensions of length, width, and thickness. The UAM process parameters and sample specifications are shown in Table 1.

3. EXPERIMENTAL SETUP AND RESULTS

Experiments were conducted on the PVDF specimen to validate its sensing capabilities while it is embedded in the metal matrix. Cantilevered and axial impact tests, and bending tests using a shaker were performed to characterize the specimen within the metal structure. These experiments relate impact loading and shaker acceleration to the sensor voltage output and strain response of the sample. It is to be noted that both unfiltered and filtered plots are shown here. A 45 dB butter-worth notch filter was applied in post processing to negate the 60 Hz hum introduced my electrical impedences.

3.1 Cantilever Impact Tests

The sample was clamped in the compressive (g_{33}) mode and subjected to impact loading at the tip to verify its impact detection and sensing performance. A strain gauge was attached at the center of the effective sensing

Downloaded From: https://www.spiedigitallibrary.org/conference-proceedings-of-spie on 23 May 2023
Terms of Use: https://www.spiedigitallibrary.org/terms-of-use

Table 1: Specimen and UAM process parameters.

Polyamide film thickness	3 layers at 50 μm
PVDF sensor total thickness	190 μm
Sonotrode	18Ni grade 350 - uncoated
Al foil thickness (H18, T4)	152 μm
Al 6061-T6 baseplate thickness	3.4 mm
Normal weld force (texture, H18, T4)	4000 N
Weld speed (texture, H18, T4)	84.67 mm/s, 84.67 mm/s, 42.33 mm/s
Weld amplitude (texture, H18, T4)	33.83 μm, 23.07 μm, 35.37 μm

area over the embedded sensor and connected to a Rigol MSO5074 oscilloscope via a signal conditioner and Wheatstone bridge to acquire the strain gauge data. The voltage output of the sensor and the impact signals were also obtained through the oscilloscope using BNC cable connections. The sample was carefully placed in the vice and held at the base of the sensing area so that it experiences maximum strain during impact (Figure 2a). A modally tuned impact hammer (PCB 086C02) was used with load sensitivity of 11.79 mV/N and a plastic tip diameter of 4.6 mm. It was applied right at the tip of the sample, 60 mm from the end of the sensing area.

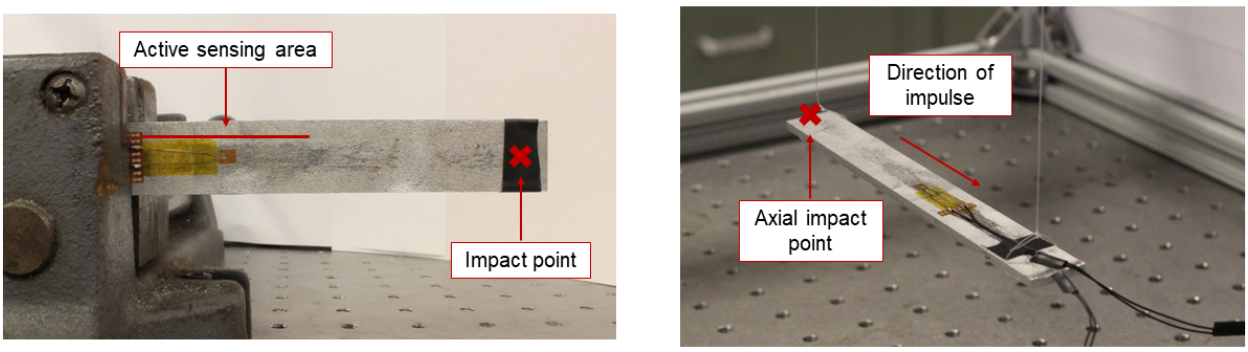

(a) (b)

Figure 2: (a) Cantilever impact test experimental setup with marked point for hammer impact. (b) Axial impact testing of the specimen hung with fishing lines from the frame.

Three tests were performed with different loading intensities in order to evaluate sensor detection capabilities and assess its repeatability. Figure 3 shows the amplitude of impact (approximately 0.3 N, 0.5 N, and 1 N, respectively) for each test and its corresponding identification by the embedded PVDF. Figure 4 shows time series plots of the PVDF voltage output which align well with the impact loadings. Furthermore, with the increase in loading amplitude, an increase in output voltage can also be observed which verifies its sensing performance under various loading conditions.

The maximum voltage output is shown in Figure 5 against the maximum impact force from the hammer, and corresponding decay in the signal validates its localization performance. An exponential fit was done using equation 1 where ζ is the damping coefficient and f_d is the damped natural frequency which can be assumed to be equal to its natural frequency (f_n = 533.3 Hz) for very small values of ζ. The decay rate comes out to be 0.13% and 0.11% for filtered and unfiltered data, respectively.

$$v(t) = e^{-2\pi\zeta f_d t} \tag{1}$$

Downloaded From: https://www.spiedigitallibrary.org/conference-proceedings-of-spie on 23 May 2023
Terms of Use: https://www.spiedigitallibrary.org/terms-of-use

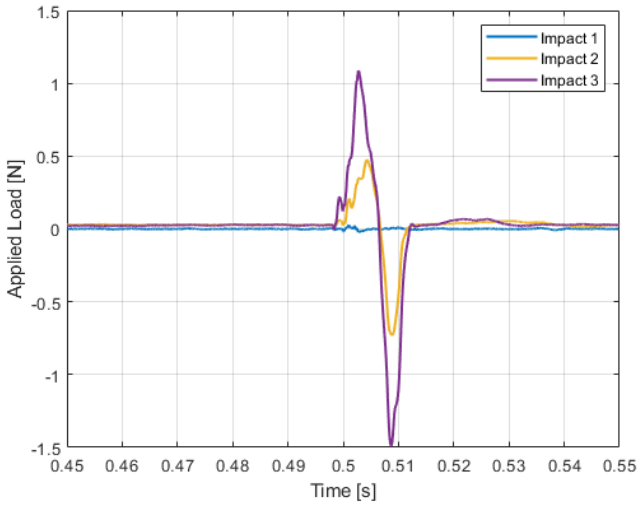

Figure 3: Impact amplitude versus time for three cantilever impact tests.

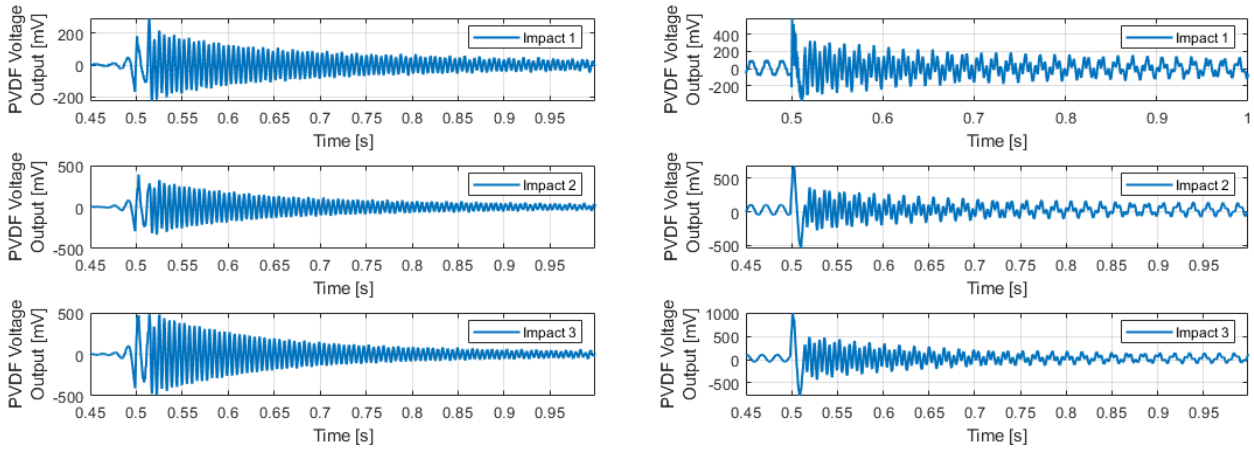

(a) (b)

Figure 4: (a) PVDF voltage output with the Butterworth notch filter applied for three cantilever impact tests. (b) Unfiltered voltage output of the embedded PVDF.

Additionally, the strain gauge output agrees with the voltage data as can be seen in Figure 6. A change in strain is observed as soon as the hammer impacts the specimen. A small delay in the strain gauge signal in comparison to impact detection of the PVDF sensor can be observed which is due to the gauge placement. The strain gauge and PVDF sensor are both centered along the sample, but the strain gauge is shorter. Therefore, the leading edge of the PVDF senses the impact first, which introduces the delay.

3.2 Axial Impact Tests

In order to ensure that no bending modes interfere with the axial test data, the sample was hung from an aluminum frame (d_{31} mode) using fishing lines which can be assumed to be massless (Figure 2b). These fishing lines were attached to the sample using loops tied around the sample and secured via Kapton tape so they do not slide when the sample is impacted axially. Similar connections were made for both the strain gauge and the sensor as well as the impact hammer as previously stated to ensure accuracy of the data acquired. The sample

Downloaded From: https://www.spiedigitallibrary.org/conference-proceedings-of-spie on 23 May 2023
Terms of Use: https://www.spiedigitallibrary.org/terms-of-use

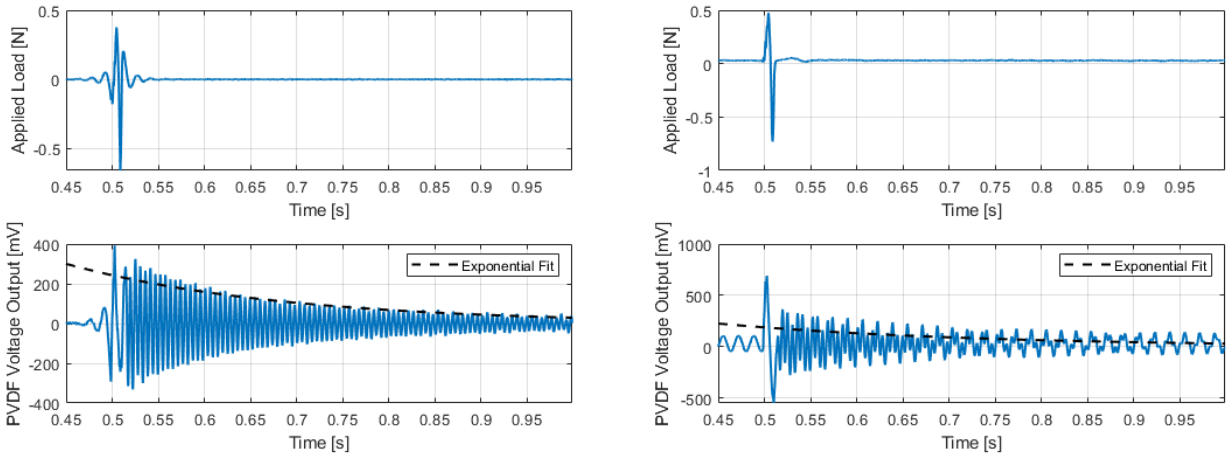

(a) (b)

Figure 5: (a) Applied load from the impact hammer and PVDF voltage output with a Butterworth notch filter applied, along with an exponential fit of the maximum PVDF voltage for Impact 2. (b) Unfiltered applied load and PVDF voltage output, along with an exponential fit of the maximum PVDF voltage.

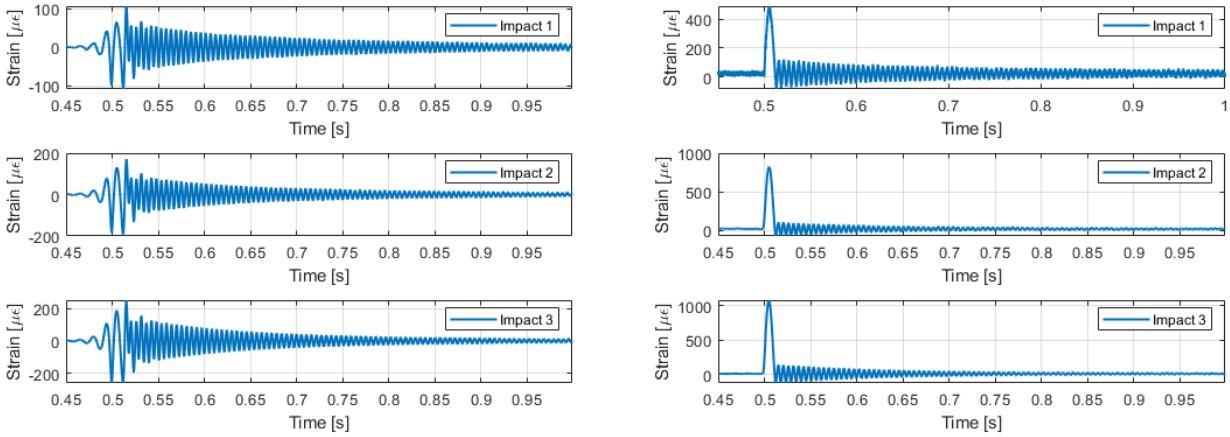

(a) (b)

Figure 6: (a) Strain output with the Butterworth notch filter applied for three cantilever impact tests. (b) Unfiltered strain output.

was impacted axially at the end opposite to the wire channel, and the corresponding PVDF voltage output and strain were measured.

Six axial tests were conducted to observe repeatability of the sensor output from the embedded PVDF. Impulses of different magnitudes were imparted to the sample and the voltage outputs from the sensor were monitored. Output from one of the tests is shown in Figure 7. Voltage output of the sensor remains minimal before the impact is made and rises proportionally as soon as the impulse is provided. A very slight delay between the impulse and voltage detection can be observed due to the time the stress waves take to travel from the end of the sample to the leading edge of the PVDF.

Downloaded From: https://www.spiedigitallibrary.org/conference-proceedings-of-spie on 23 May 2023
Terms of Use: https://www.spiedigitallibrary.org/terms-of-use

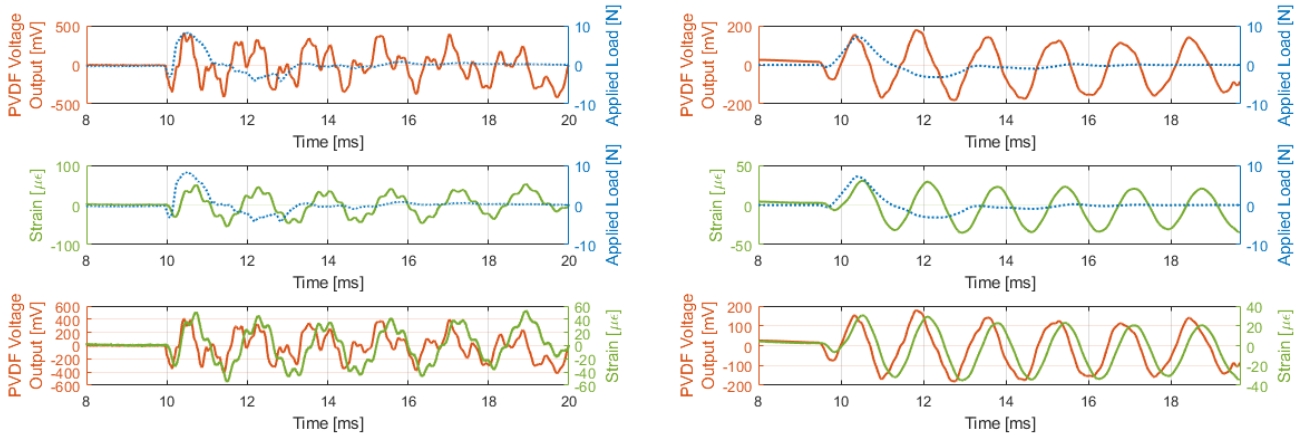

(a) (b)

Figure 7: (a) PVDF voltage output and strain plotted against impact load with a Butterworth notch filter applied. (b) Unfiltered PVDF voltage and strain plotted against impact load.

Maximum voltage output by the sensor is plotted against the maximum impulse detected and curve fitted to quantify sensor sensitivity. The linear fit has a coefficient of determination (R^2) of 97.7% which verifies the goodness of fit and the proportionality of voltage output with impulse amplitude. Additionally, sensitivity of the sensor is quantified to be 43.7 mV/N which shows the change in voltage output per unit of impulse amplitude. A sensor with a higher sensitivity can detect minor changes in input and is preferred over less sensitive sensors.[25] This shows that the embedded sensor can indeed detect changes in impulse forces and hence validates its sensing capability.

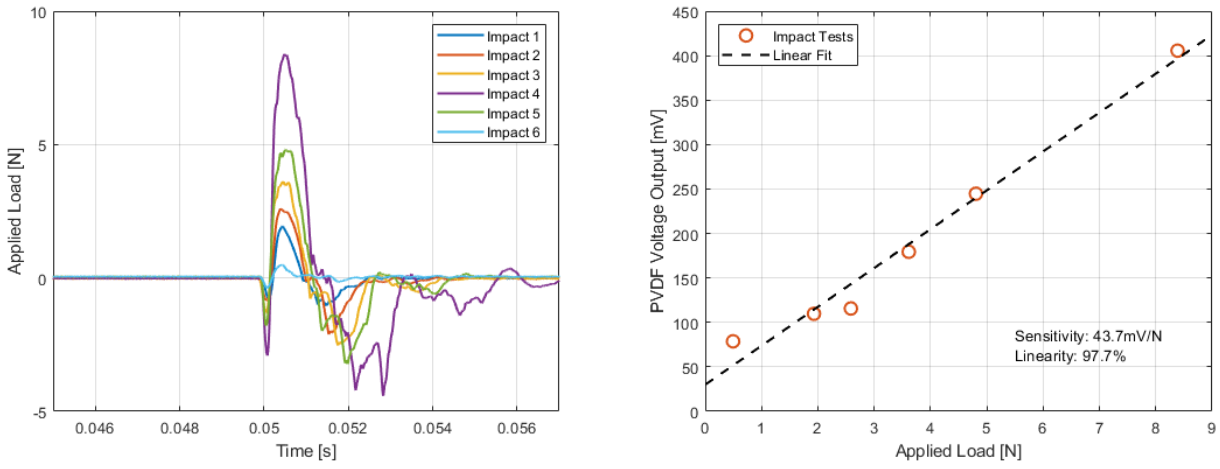

(a) (b)

Figure 8: (a) Impact load for the six axial impact tests conducted. (b) Measured impulse force amplitude vs the amplitude of PVDF voltage response. The dashed black line represents the linear fit model of the measurement.

Downloaded From: https://www.spiedigitallibrary.org/conference-proceedings-of-spie on 23 May 2023
Terms of Use: https://www.spiedigitallibrary.org/terms-of-use

3.3 Bending Tests

An ET 126-1 25 lbf Labworks shaker was used to impart excitation to the sample which was hung from a support frame at the wire channel end using fishing lines. A 150 mm long 6-32 threaded 6061 aluminum rod was used as a stinger to avoid creating any moments in the horizontally aligned shaker. A clamp was 3D printed with PLA using an Ultimaker S5 to latch onto the stinger and firmly grip the sample. It was ensured to have a snug fit to prevent slipping along the sample during the shaker excitation. Connections were made as described previously and data was recorded using the oscilloscope.

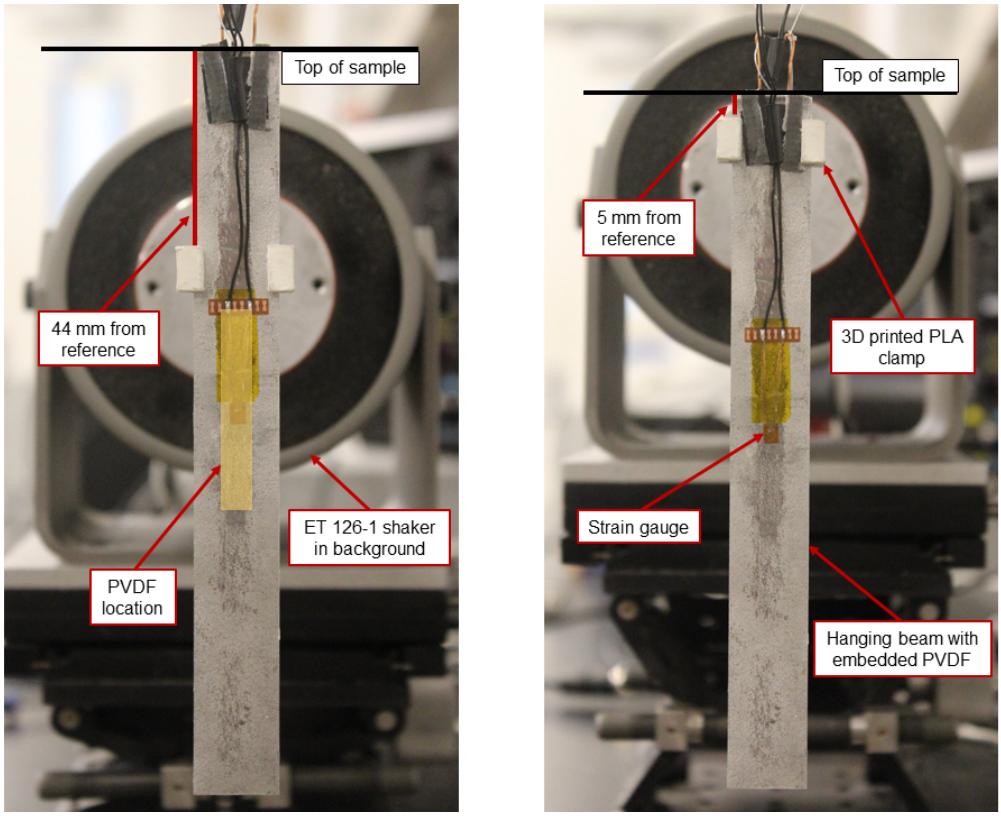

(a) (b)

Figure 9: Bending (shaker) test setup: (a) beam clamped 44 mm from the top, (b) beam clamped 5 mm from the top.

The clamp on the sample was placed in two positions: 44 mm and 5 mm from the top, as displayed in Figure 9. A 1 Hz to 1 kHz frequency sweep was performed with an applied input of 10 V and data was acquired to observe voltage output from the sensor. The power spectrum of the voltage output data is shown in Figure 10. It can be observed that the PVDF outputs maximum voltage at the resonance which is 533.33 Hz and 481.35 Hz for clamping position 1 (Figure 10a) and position 2 (Figure 10b), respectively. An initial peak at 60 Hz can be seen in both plots which is electrical noise in the unfiltered data. Both clamping positions display similar results with only an expected decrease in resonance from position 1 to position 2 due to the increase in effective length of the vibrating beam.

Using a simplified Euler-Bernoulli two span beam model with free-pinned-free support, natural frequency of the beam was calculated for both clamping positions based on the following assumptions:

- The beam was isolated from the setup and assumed to be representated by a linear, uniform, homogeneous, and isotropic elastic beam.

Downloaded From: https://www.spiedigitallibrary.org/conference-proceedings-of-spie on 23 May 2023
Terms of Use: https://www.spiedigitallibrary.org/terms-of-use

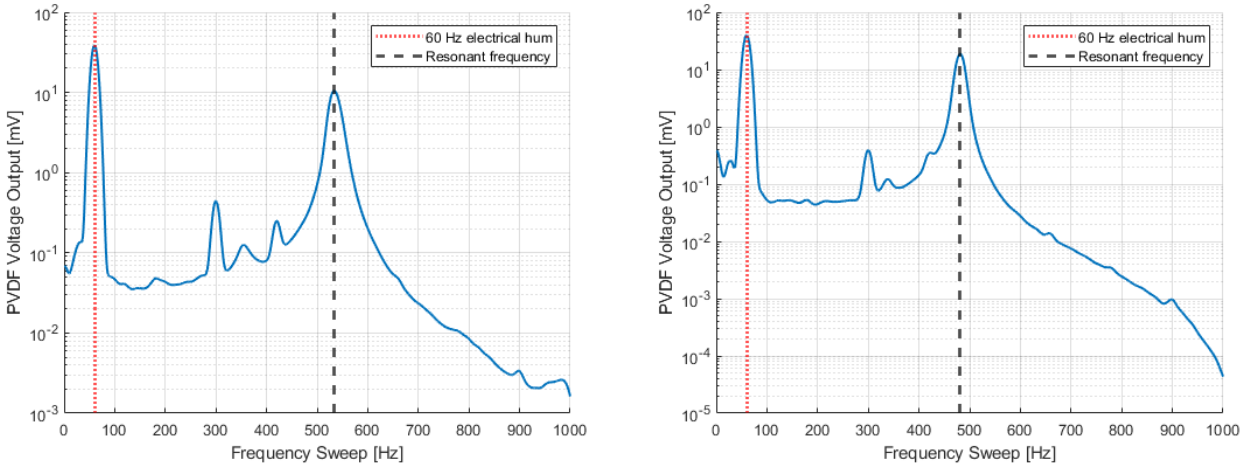

(a) (b)

Figure 10: frequency sweep of the voltage output from 1 Hz - 1 kHz: (a) Beam clamped 44 mm from the top. (b) Beam clamped 5 mm from the top.

- Mass of the stinger rod was taken to be negligible and therefore plays no part in the calculations.
- The clamp attaching the stinger to the beam was assumed to be a pinned support at that position with no other effect on the beam as a whole.
- Properties of Al 6061-T6 were assumed for the whole beam, neglecting any differences due to 6061-H18 and 6061-T4 foils.
- The machined pocket for PVDF embedment was taken to be a regular rectangular shaped slot with depth equivalent to the depth of the deepest pocket for calculation of area moment of inertia.
- The PVDF sensor and surface strain sensor have very low stiffnesses compared to the beam and therefore do not contribute much to the overall natural frequency.

Thus, utilising the following natural frequency formula presented by Blevins,[26] we have:

$$f_i = \frac{\lambda_i^2}{2\pi L^2}\sqrt{\frac{EI}{\rho A}} \tag{2}$$

where E = elastic modulus of Al 6061-T6, I = second area moment of inertia, ρ = density of Al 6061-T6, A = area of beam cross-section, L = characteristic length of the beam, and λ_i is a dimensionless parameter which is a function of the boundary conditions (λ_1 corresponds to the first vibrational mode based on the length ratio of both spans given by Blevins[26]).

Using the parameters in Table 2 and substituting in equation 2, we have $f_{1,position1}$ = 558.7 Hz and $f_{1,position2}$ = 509.1 Hz, respectively. These represent percentage errors of 4.76% and 5.77%, respectively, relative to the experimental measurements, which can be mainly attributed to the fact that the beam has an embedded sensor and internal features which are not accounted for, the wires for the PVDF sensor are extending out of the end, and the stinger is not attached to the beam at a point by a pin joint, among other assumptions. However, these natural frequencies calculated can be seen to agree with the experimental resonances obtained and correspondingly, the maximum voltage output from the embedded PVDF. Thus, these results validate the sensing capabilities of the embedded sensor under bending (shaker) tests which can be utilized for practical applications in non-destructive evaluation (NDE) approaches for structural health monitoring (SHM) purposes.

Downloaded From: https://www.spiedigitallibrary.org/conference-proceedings-of-spie on 23 May 2023
Terms of Use: https://www.spiedigitallibrary.org/terms-of-use

Table 2: Beam parameters for natural frequency calculation.

Elastic modulus (E)	68.9 GPa
Density (ρ)	2700 kg/m^3
Width of beam (b)	19.05 mm
Thickness of beam (h)	3.4 mm
λ_1 for position 1	4.4
λ_1 for position 2	4.2

4. CONCLUDING REMARKS

This article details the functional performance of an embedded PVDF sensor and characterizes its sensing capabilities through experimentation. It presents a process for fabrication of an embedded piezoelectric sensor in an aluminum structure using ultrasonic additive manufacturing (UAM). The sensor is tacked lightly into a machined pocket and is pre-compressed by welding aluminum foils on top of it to enhance the mechanical coupling of the embedded PVDF sensor with the metal matrix. Impact and bending tests were conducted on the manufactured sample and its sensing performance was discussed. The embedded sensor displayed a steady decay rate when impacted in the g_{33} mode in the cantilevered configuration. Additionally, it exhibited a sensitivity of 43.7 mV/N under axial impulses (d_{31} mode) while displaying high linearity within six impact tests. Finally, bending tests using a shaker displayed a maximum voltage output from the PVDF under resonance of the beam which demonstrates the effectiveness of the embedded sensor and its sensing capabilities for structural vibration monitoring. This fabrication methodology for embedding active materials can prove beneficial for many applications in tactile sensing and structural health monitoring which provides directions for future work in intelligent adaptive systems.

ACKNOWLEDGMENTS

We wish to acknowledge the member organizations of the Smart Vehicle Concepts Center, a Phase III National Science Foundation Industry-University Cooperative Research Center under grant NSF IIP 1738723 (http://www.SmartVehicleCenter.org). Any opinions, findings, and conclusions or recommendations expressed in this material are those of the authors and do not necessarily reflect the views of the National Science Foundation.

REFERENCES

[1] Kumar, A., "Methods and materials for smart manufacturing: Additive manufacturing, internet of things, flexible sensors and soft robotics," *Manufacturing Letters* **15**, 122–125 (2018). Industry 4.0 and Smart Manufacturing.

[2] Karnik, N., Bora, U., Bhadri, K., Kadambi, P., and Dhatrak, P., "A comprehensive study on current and future trends towards the characteristics and enablers of industry 4.0," *Journal of Industrial Information Integration* **27**, 100294 (2022).

[3] Javaid, M., Haleem, A., Singh, R. P., Rab, S., and Suman, R., "Significance of sensors for industry 4.0: Roles, capabilities, and applications," *Sensors International* **2**, 100110 (2021).

[4] Hu, B., Kundu, T., Grill, W., Liu, B., and Toufigh, V., "Embedded piezoelectric sensors for health monitoring of concrete structures," *ACI Materials Journal* **110**, 149–158 (03 2013).

[5] Gayakwad, H. and Thiyagarajan, J. S., "Structural damage detection through emi and wave propagation techniques using embedded pzt smart sensing units," *Sensors* **22**(6) (2022).

[6] Wang, Z., Wei, L., and Cao, M., "Damage quantification with embedded piezoelectric aggregates based on wavelet packet energy analysis," *Sensors* **19**(2) (2019).

[7] Paradies, R. and Ruge, M., "In situ fabrication of active fibre reinforced structures with integrated piezoelectric actuators," *Smart Materials and Structures* **9**, 220 (Apr 2000).

Downloaded From: https://www.spiedigitallibrary.org/conference-proceedings-of-spie on 23 May 2023
Terms of Use: https://www.spiedigitallibrary.org/terms-of-use

[8] Schulze, R., Streit, P., Fischer, T., Tsapkolenko, A., Heinrich, M., Sborikas, M., Kroll, L., Gessner, T., and Wegener, M., "Fiber-reinforced composite structures with embedded piezoelectric sensors," in [*SENSORS, 2014 IEEE*], 1563–1566 (2014).
[9] Hornig, A., Frohberg, R., Bätzel, T., Gude, M., and Modler, N., "Embedded sensing and actuating in cfrp composite structures—concept and technology demonstration for tailored embeddable sensor-actuator layers (TEmSAL)," *Smart Materials and Structures* **31**, 095007 (Jul 2022).
[10] Ghasemi-Nejhad, M. N., Russ, R., and Pourjalali, S., "Manufacturing and testing of active composite panels with embedded piezoelectric sensors and actuators," *Journal of Intelligent Material Systems and Structures* **16**(4), 319–333 (2005).
[11] Grandal, T., Zornoza, A., López, A., Fraga, S., Sun, T., and Grattan, K. T. V., "Analysis of fiber optic sensor embedded in metals by automatic and manual TIG welding," *IEEE Sensors Journal* **19**(17), 7425–7433 (2019).
[12] Hossain, M. S., Gonzalez, J. A., Hernandez, R. M., Shuvo, M. A. I., Mireles, J., Choudhuri, A., Lin, Y., and Wicker, R. B., "Fabrication of smart parts using powder bed fusion additive manufacturing technology," *Additive Manufacturing* **10**, 58–66 (2016).
[13] Britto, J. J. J. and Vasanthanathan, A., "Smart piezo-bonded carbon fibre/epoxy composite structure: experiments and finite element simulation," *Materials Research Express* **9**, 045702 (Apr 2022).
[14] Karayannis, C. G., Golias, E., Naoum, M. C., and Chalioris, C. E., "Efficacy and damage diagnosis of reinforced concrete columns and joints strengthened with FRP ropes using piezoelectric transducers," *Sensors* **22**(21) (2022).
[15] Shen, Z., Zhang, Z., Zhang, N., Li, J., Zhou, P., Hu, F., Rong, Y., Lu, B., and Gu, G., "High-stretchability, ultralow-hysteresis conductingpolymer hydrogel strain sensors for soft machines," *Advanced Materials* **34**(32), 2203650.
[16] Madhavan, R., "Network crack-based high performance stretchable strain sensors for human activity and healthcare monitoring," *New J. Chem.* **46**, 17596–17609 (2022).
[17] Han, L., Wang, X., and Sun, Y., "The effect of bonding layer properties on the dynamic behaviour of surface-bonded piezoelectric sensors," *International Journal of Solids and Structures* **45**(21), 5599–5612 (2008).
[18] Ramanathan, A. K., Gingerich, M. B., Headings, L. M., and Dapino, M. J., "Metal structures embedded with piezoelectric PVDF sensors using ultrasonic additive manufacturing," *Manufacturing Letters* **31**, 96–100 (2022).
[19] Friel, R. and Harris, R., "Ultrasonic additive manufacturing – a hybrid production process for novel functional products," *Procedia CIRP* **6**, 35–40 (2013). Proceedings of the Seventeenth CIRP Conference on Electro Physical and Chemical Machining (ISEM).
[20] [*Smart Structure Integration Through Ultrasonic Additive Manufacturing*], *Smart Materials, Adaptive Structures and Intelligent Systems* **2** (09 2014).
[21] Kong, C., Soar, R., and Dickens, P., "Ultrasonic consolidation for embedding sma fibres within aluminium matrices," *Composite Structures* **66**(1), 421–427 (2004). Twelfth International Conference on Composite Structures.
[22] Li, J., Monaghan, T., Nguyen, T., Kay, R., Friel, R., and Harris, R., "Multifunctional metal matrix composites with embedded printed electrical materials fabricated by ultrasonic additive manufacturing," *Composites Part B: Engineering* **113**, 342–354 (2017).
[23] Hyer, H. C., Sweeney, D. C., and Petrie, C. M., "Functional fiber-optic sensors embedded in stainless steel components using ultrasonic additive manufacturing for distributed temperature and strain measurements," *Additive Manufacturing* **52**, 102681 (2022).
[24] Hahnlen, R. and Dapino, M., "Active metal-matrix composites with embedded smart materials by ultrasonic additive manufacturing," *Proceedings of SPIE - The International Society for Optical Engineering* **7645**, 15– (03 2010).
[25] Vig, J. and Walls, F., "A review of sensor sensitivity and stability," in [*Proceedings of the 2000 IEEE/EIA International Frequency Control Symposium and Exhibition (Cat. No.00CH37052)*], 30–33 (2000).
[26] Blevins, R. D., [*Formulas for natural frequency and mode shape*], Van Nostrand Reinhold Co New York (1979).

Downloaded From: https://www.spiedigitallibrary.org/conference-proceedings-of-spie on 23 May 2023
Terms of Use: https://www.spiedigitallibrary.org/terms-of-use